

Supplementary Material for “Photometric Stereo via Discrete Hypothesis-and-Test Search”

1. Visualization of the varying light distributions

On Page 5 of the main paper, we described 5 light distributions comprised of 20, 40, 60, 80, 100 lights, respectively. The light distributions are generated by a generalized spiral points algorithm [4]. Our 5 distributions are illustrated in Fig. 1.

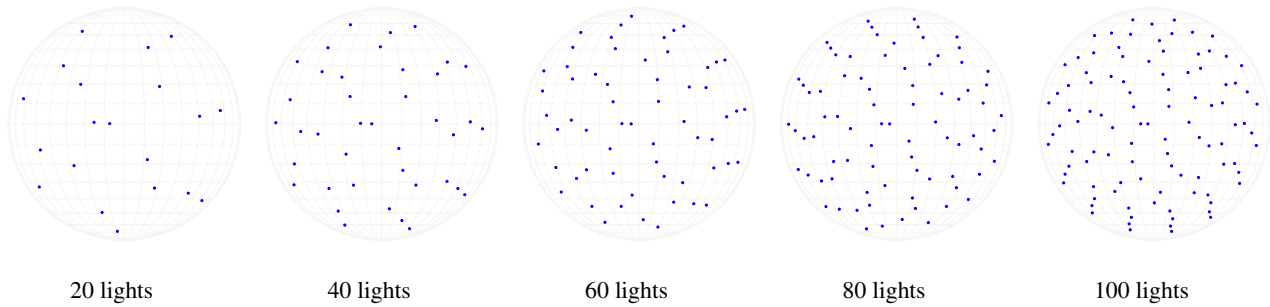


Figure 1: Light distributions.

2. Details of 5-fold cross-validation

On Page 6 of the main paper, we described that we split the 100 MERL BRDFs into 5 groups for 5-fold cross-validation. The exact grouping is summarized in Table 1.

Table 1: 5 groups of MERL BRDFs for the cross-validation.

Group 1	Group 2	Group 3	Group 4	Group 5
color-changing-paint1	colonial-maple-223	green-latex	pure-rubber	white-fabric2
violet-rubber	color-changing-paint2	ss440	chrome	green-metallic-paint2
grease-covered-steel	dark-blue-paint	delrin	polyethylene	brass
silver-metallic-paint	black-obsidian	gold-paint	teflon	pvc
specular-green-phenolic	yellow-matte-plastic	specular-orange-phenolic	natural-209	white-fabric
alum-bronze	silicon-nitride	yellow-phenolic	beige-fabric	yellow-paint
white-diffuse-bball	red-plastic	specular-maroon-phenolic	specular-yellow-phenolic	white-paint
green-acrylic	blue-acrylic	nickel	blue-metallic-paint	pink-felt
pearl-paint	ipswich-pine-221	violet-acrylic	cherry-235	red-metallic-paint
pink-fabric2	gray-plastic	green-plastic	nylon	hematite
red-fabric2	alumina-oxide	white-marble	specular-black-phenolic	specular-blue-phenolic
black-fabric	maroon-plastic	silver-metallic-paint2	yellow-plastic	gold-metallic-paint2
neoprene-rubber	special-walnut-224	aluminium	red-fabric	blue-metallic-paint2
light-brown-fabric	specular-white-phenolic	green-fabric	fruitwood-241	black-soft-plastic
orange-paint	pink-jasper	gold-metallic-paint3	white-acrylic	blue-rubber
light-red-paint	steel	gold-metallic-paint	specular-red-phenolic	two-layer-silver
black-oxidized-steel	pink-fabric	pickled-oak-260	specular-violet-phenolic	two-layer-gold
silver-paint	chrome-steel	green-metallic-paint	aventurine	blue-fabric
polyurethane-foam	tungsten-carbide	dark-red-paint	color-changing-paint3	pink-plastic
dark-specular-fabric	red-specular-plastic	black-phenolic	red-phenolic	purple-paint

3. Additional visual comparisons on the Stanford bunny with spatially-varying materials

In Figures 2 and 3, we show estimated surface normals and their angular error maps for the Stanford bunny rendered with 5 distinct sets of materials, comparing our method with CNN-based [2], model-based [3], dictionary-based [1] methods.

On all datasets, our method consistently outperforms the CNN-based and model-based methods on the mean/variance of angular errors. Neither our method nor the dictionary-based method outperforms the other on all datasets, showing that the end of development of data-based photometric stereo has not been reached yet.

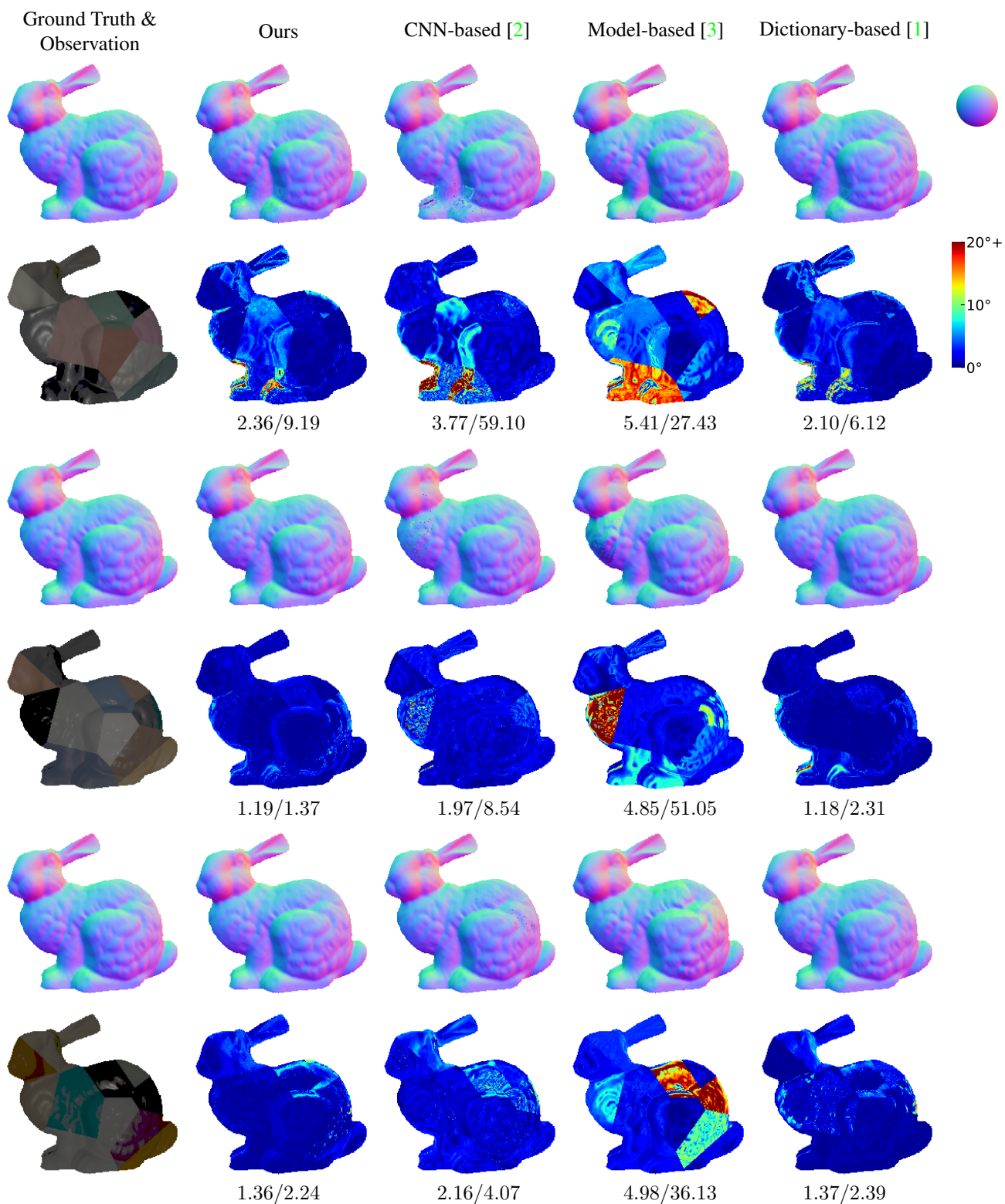


Figure 2: Visual comparisons on the Stanford bunny with spatially-varying material part (1). We show the estimated surface normals and angular error maps of our method, a CNN-based method [2], a model-based method [3], and a dictionary-based method [1]. The numbers under the angular error maps show mean/variance of the angular errors.

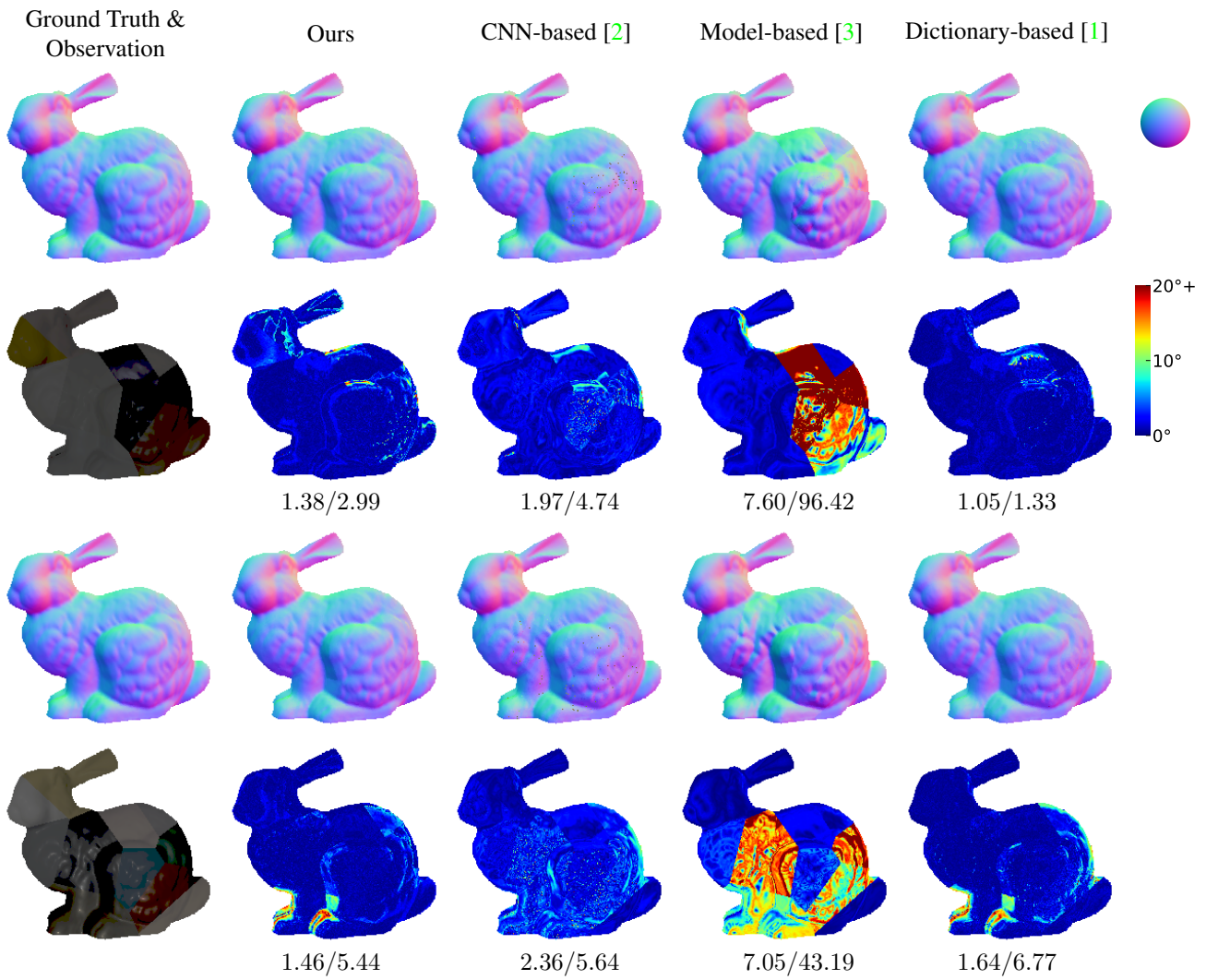


Figure 3: Visual comparisons on the Stanford bunny with spatially-varying material part (2). See explanations in the caption of Fig. 2.

4. Additional visual comparisons on the DiLiGenT dataset

In Figures 4 and 5, we show estimated surface normals and their angular error maps for all ten objects from the DiLiGenT dataset [5], comparing our method with a CNN-based method [2].

As described in the main paper, our method shows greater angular errors in pixels where cast shadows or inter-reflections are present. For instance, the errors at the bottom of each object are likely caused by reflections from the floor. On the other hand, in convex parts where inter-reflections or cast shadows do not occur, our method yields better accuracy than the CNN-based state-of-the-art method, not only for diffuse materials but also for complex specular or metallic materials, *e.g.*, for the Ball, Buddha, Cow, Harvest and Reading scenes.

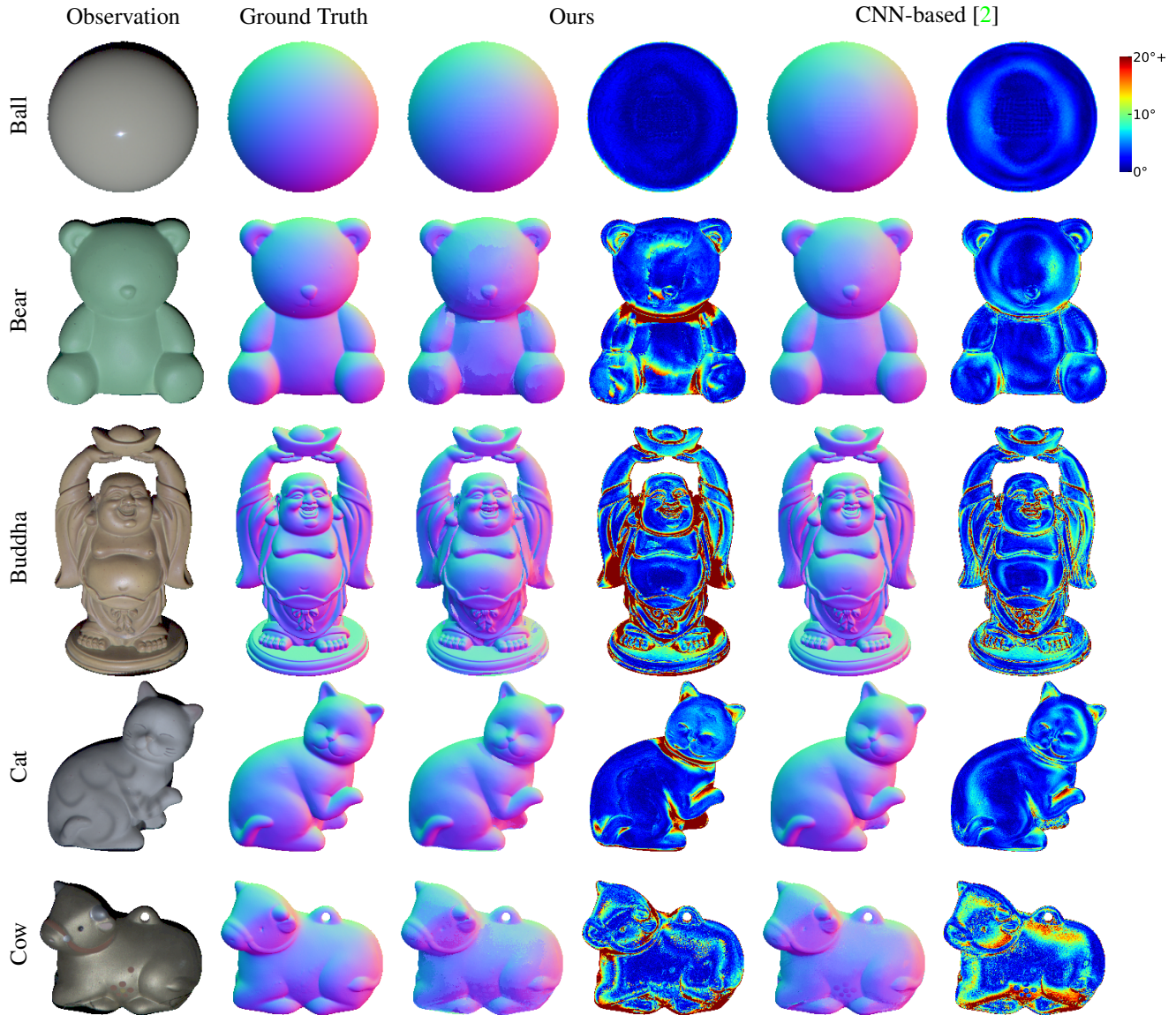


Figure 4: Visual comparisons of our method and a CNN-based method [2] on the DiLiGenT dataset part (1). We show estimated surface normals and angular error maps of our method and the CNN-based method.

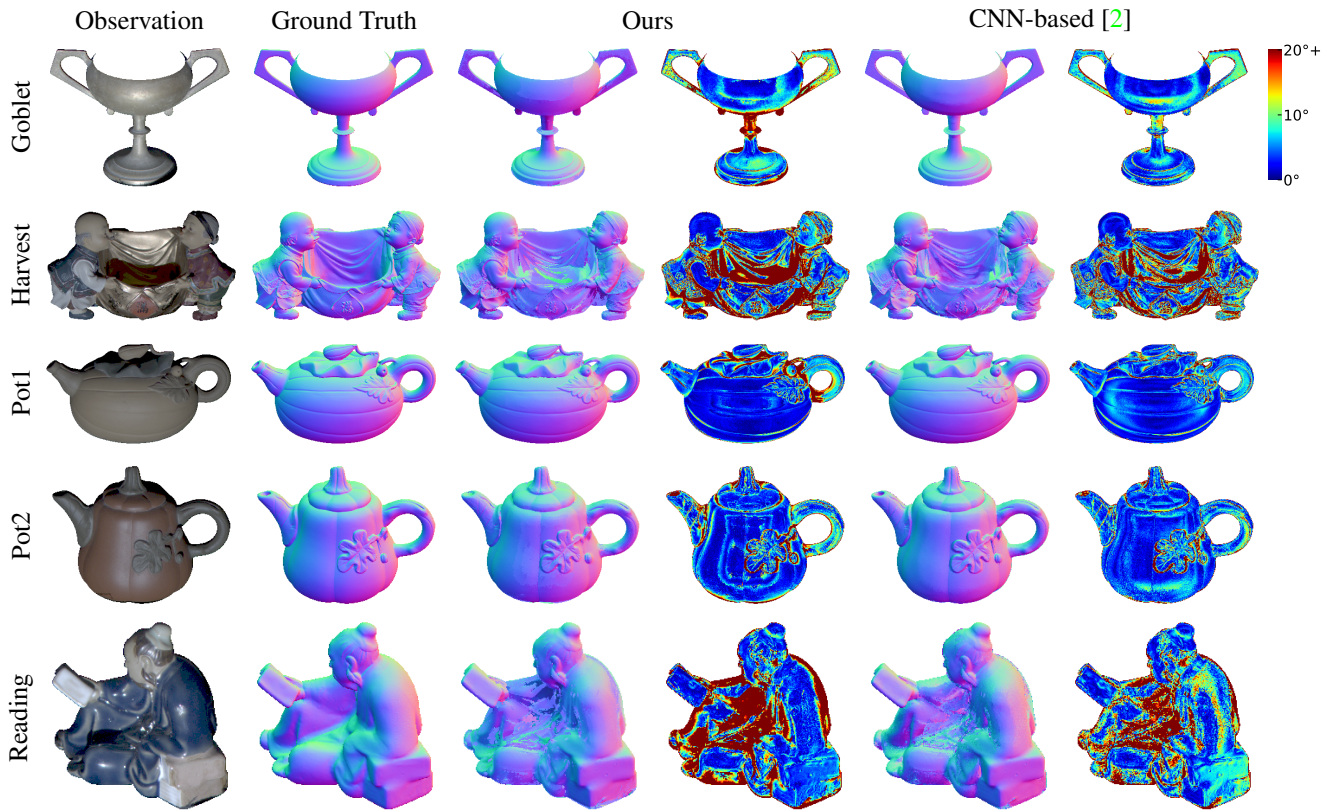


Figure 5: Visual comparisons of our method and a CNN-based method [2] on the DiLiGenT dataset part (2). We show estimated surface normals and angular error maps of our method and the CNN-based method.

References

- [1] Zhuo Hui and Aswin C. Sankaranarayanan. Shape and spatially-varying reflectance estimation from virtual exemplars. *Transactions on Pattern Analysis and Machine Intelligence (PAMI)*, 39(10):2060–2073, 2017. [2](#), [3](#), [4](#)
- [2] Satoshi Ikehata. CNN-PS: CNN-based photometric stereo for general non-convex surfaces. In *European Conference on Computer Vision (ECCV)*, 2018. [2](#), [3](#), [4](#), [5](#), [6](#)
- [3] Satoshi Ikehata and Kiyoharu Aizawa. Photometric stereo using constrained bivariate regression for general isotropic surfaces. In *Computer Vision and Pattern Recognition (CVPR)*, 2014. [2](#), [3](#), [4](#)
- [4] Edward B. Saff and Arno Kuijlaars. Distributing many points on a sphere. *The Mathematical Intelligencer*, 19(1):5–11, 1997. [1](#)
- [5] Boxin Shi, Zhipeng Mo, Zhe Wu, Dinglong Duan, Sai-Kit Yeung, and Ping Tan. A benchmark dataset and evaluation for non-Lambertian and uncalibrated photometric stereo. *Transactions on Pattern Analysis and Machine Intelligence (PAMI)*, 41(2):271–284, 2019. [5](#)